Facies (2004) 50:113–131
DOI 10.1007/s10347-004-0003-z

ORIGINAL ARTICLE

Boris Kostic · Thomas Aigner

Sedimentary and poroperm anatomy of shoal-water carbonates (Muschelkalk, South-German Basin): an outcrop-analogue study of inter-well spacing scale

Received: 28 April 2003 / Accepted: 18 January 2004 / Published online: 10 March 2004

Abstract Outcrop-analogue studies are rarely carried out on a very detailed scale of just several hundred metres, which represents a common inter-well spacing. Superb outcrop conditions in south Germany for Upper Muschelkalk shoal-water carbonates located on a carbonate ramp allowed us to perform a detailed analysis of their sedimentary and poroperm organisation. The cyclic structure of the carbonates is evident in three types of genetic sequences 1–3 m thick, which in turn build larger-scale sequences. Lateral variations of microfacies in the study area are restricted to a few percent of individual components, leading to an excellent degree of correlation of sequences. Microfacies do not correlate well with porosity and permeability. Therefore, in order to characterise reservoir properties of the carbonate-sand shoal it is necessary to integrate rock fabric and pore type. The cyclic framework outlined in this outcrop analogue provides a predictive tool for subsurface reservoir characterisation. The stratigraphic sequences correspond to fluid-flow units showing the thickest (up to 2 m) and best reservoir qualities (ϕ up to 20%, *k* up to 53 md) towards the overall regressive maximum.

Keywords Carbonate shoal · Genetic sequence · Porosity · Permeability · Outcrop analogue · Upper Muschelkalk · German Basin

Introduction

Goal

The goal of this study is an analysis of the sedimentary and petrophysical structure of a carbonate-sand shoal on a local scale. The shoal was traced laterally for approximately 1300 m, which represents a common inter-well spacing that is seldom covered by detailed sedimentological and petrophysical data. The well-exposed shoal deposits serve as an outcrop analogue for subsurface reservoirs of similar origin (for instance in the Khuff, Hanifa, and Arab Formations of the Middle East), which are major exploration targets for oil and gas production. This study is embedded in a broader outcrop-analogue project that deals with the regional-scale characterisation (kilometres to tens of kilometres) of carbonate-sand bodies in the Upper Muschelkalk of south Germany (Braun 2003; Ruf 2001).

Methods

Using concepts of dynamic stratigraphy (Aigner et al. 1999; Matthews 1984), four outcrop sections were examined from small (microfacies analysis) to large scale (architectural, sequence, and stacking analyses) (Fig. 1). Facies analysis was based upon microscopic analysis of

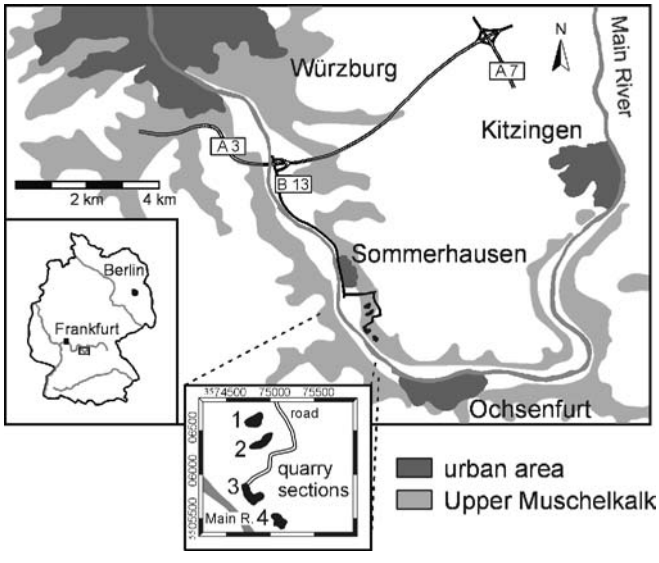

Fig. 1 Location of the study area. Enlargement shows the site of the quarry sections with Gauss-Krüger coordinates

B. Kostic · T. Aigner (✉)
Institute of Geosciences,
University of Tübingen,
Sigwartstrasse 10, 72076 Tübingen, Germany
e-mail: thomas.aigner@uni-tuebingen.de
Tel.: +49-7071-2975923
Fax: +49-7071-295727

polished slabs and thin sections combined with macroscopic field logging. The spatial distribution of primary sedimentary structures was mapped along outcrop walls and was documented with photographs. Paleocurrent data was measured on three-dimensional exposures. Outcrop gamma-ray measurements were carried out using a portable gamma-ray total-count instrument (GB-H 1635). The measuring time was 10 s at 10 cm vertical intervals for all four outcrop sections.

Quantitative porosity and permeability measurements were carried out in the laboratory on more than 140 plug samples (40 mm length and diameter) drilled from rock samples collected from all four outcrops at vertical intervals of 10–20 cm, focusing on the lowest three sequences. Porosity was determined with a powder and a helium pycnometer (Micromeritics GeoPyc 1360 and AccuPyc 1330), which measure the envelope volume and net volume of the sample respectively. Permeability was measured with a gas mini-permeameter (FPP 300 Edinburgh Petroleum Services). Air was injected into the sample with a pressure of 1.2 bar and air flow rate was measured. By pressing the injection head onto the fixed sample with a constant pressure of 3 bar, leakage around the sample was minimised. Four measurements were taken from every plug sample along and perpendicular to the axis of the cylindrical plug respectively, and horizontal and vertical permeabilities were calculated from the arithmetic mean of the measurement results. In outcrop 4 the poroperm distribution was visually mapped along one quarry wall (22 m long, 2 m thick) and supported by quantitative measurements of selected samples.

General setting

During Upper Muschelkalk times (late Anisian and Ladinian) the German Basin was a semi-enclosed intracratonic basin connected with the Tethys ocean through several seaways (Fig. 2a). A gently inclined carbonate ramp similar to the modern Persian Gulf developed northwest of the Vindelician-Bohemian High (Aigner 1985). This paleohigh delivered clastic sediments which were deposited in a zone parallel to the ancient coastline (Schröder 1967). Further seaward, this zone passed into a lagoonal environment characterised by black pebbles, oncoids, and abundant trace fossils. The lagoon with partly dolomitic rocks was separated from the argillaceous limestones of the basinal area by a belt of oolitic and bioclastic carbonate sands (Fig. 2b). These high-energy sediments represent the carbonate shoal complex.

Stratigraphic subdivision in the Upper Muschelkalk of south Germany is based on lithostratigraphic marker beds as well as on biostratigraphy using ceratites (e.g. Urlichs 1993), ostracods, and conodonts (Kozur 1974). Lithostratigraphic markers are either thin argillaceous limestone horizons ("Tonhorizonte") or bioclastic marker beds. The stratigraphic interval relevant to this study extends from the "Unterer Hauptquaderhorizont" to the "Glaukonitbank", which therefore covers the uppermost part of the

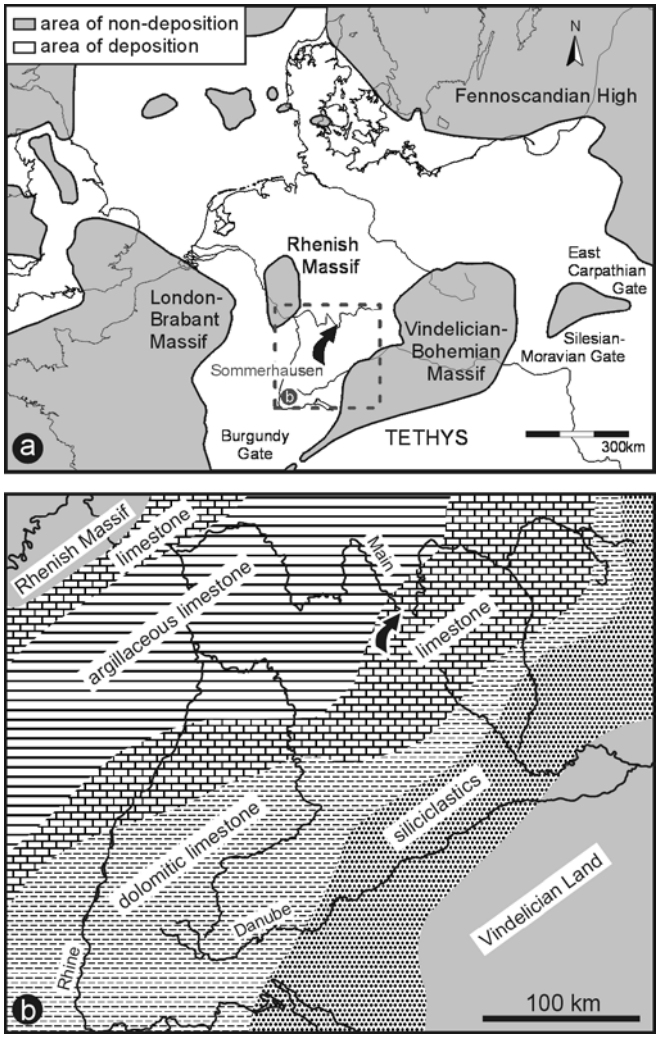

Fig. 2 **a** Paleogeography of the Upper Muschelkalk in central Europe (after Ziegler 1990). **b** Generalized map of major facies belts in the South-German Basin for the upper part of the Upper Muschelkalk (Ladinian) (after Aigner 1985). The arrow points to the location of the study area

Upper Muschelkalk (Ladinian) (Fig. 3). An English translation of the stratigraphic terms has not been attempted, since there is already some confusion about the German nomenclature.

Facies and sequences

Microfacies

Various microfacies types are classified based on lithology, texture, sorting, frequency and composition of allochems, and sedimentary structures. Facies descriptions and interpretations are summarised in the accompanying facies chart (Table 1); the most frequently occurring microfacies types are illustrated in Fig. 4. On the basis of these interpretations, the lateral facies distribution along the carbonate ramp is reconstructed extending from

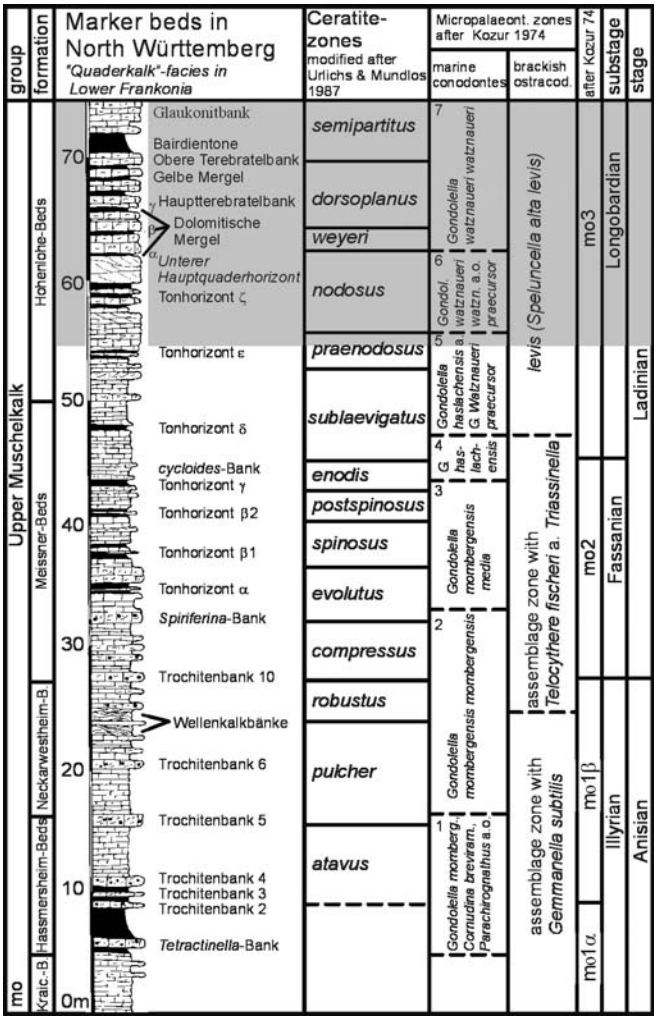

Fig. 3 Stratigraphy of the Upper Muschelkalk (after Hagdorn 1991). Relevant section for the study area is marked in grey

a high-energy shoal facies to a storm-dominated offshoal area (Fig. 5).

Genetic sequences

The analysis of the vertical succession of microfacies types clearly shows a cyclic organisation. This cyclic structure is also evident in outcrop gamma-ray measurements. According to the base-level concept of Wheeler (1964) and Cross and Lessenger (1998), three characteristic types of stratigraphic cycles are recognised. The base-level concept applied here expresses the relationship between accommodation and sediment supply and their relative change throughout the stratigraphic succession. A complete base-level cycle consists of a base-level-fall hemicycle showing a decreasing accommodation/supply ratio followed by a base-level-rise hemicycle showing an increasing accommodation/supply ratio. The turnaround points between the hemicycles are represented either by surfaces of stratigraphic discontinuity or by conformable strata. The smallest stratigraphic unit that is regionally traceable and contains the sediments which accumulated during a full base-level cycle forms the fundamental unit of the stratigraphic succession. As these units in the present case contain rise and fall hemicycles, they are not referred to as parasequences. Instead, following Busch (1959), Homewood et al. (1992) and Homewood et al. (2000), such a unit is referred to as a "genetic sequence" or "genetic unit". In the following, the idealised genetic sequences identified in the study area are described. Continuous transitions are recognised between the different types of genetic sequences.

Shoal complex genetic sequence

Description: This succession generally reaches 2–3 m in thickness (Fig. 6a) and starts with lime mudstone, commonly including intercalated argillaceous lime mudstone. These are overlain by arenitic bioclastic mud-lean packstones showing an erosive base, and parallel subhorizontal lamination which passes locally into climbing ripples (Fig. 7a). The ripple sets are truncated by subsequent sets displaying an upward decrease in grain size. This kind of stratification is equivalent to the upper zone of an idealised hummocky sequence described by Dott and Bourgeois (1982). Amalgamated hummocky cross-stratification with typical swales and hummocks is present in only a few locations (Fig. 7b). The main part of the sequence consists of massive, cross-bedded bioclastic grainstones that occasionally contain layers of packstones. Intraclasts chiefly occur at the basal part of this unit. In general, sorting, roundness, and the proportion of micritic envelopes increase upwards. Ooids and coated grains are concentrated in the uppermost part. Trough cross-bedding representing highly amalgamated dune sets dominate, although ripple lamination also occurs (Fig. 7c, d). Mapping of the sedimentary structures reveals a lateral extent of single dunes ranging from a few metres to tens of metres, whereas their preserved thickness commonly lies in the range of 10–60 cm (Fig. 8). Typically, the set heights of the dunes increase towards the top of the unit, as well as laterally towards the south of the study area. In the southeasternmost outcrop (section 4) a sand wave with counter-flow ripples was identified (Fig. 7e–g), which is exposed laterally for more than 25 m (Fig. 9). Single cross-beds are slightly eroded. The grainstone unit is generally 1.5–2.4 m thick, and is abruptly overlain by a bioturbated wackestone a few decimetres thick, with a pronounced nodular structure and extensive fecal pellets.

Interpretation: All vertical trends within this type of sequence indicate shallowing-upward from a low-energy environment at the base, intermittent-energy storm deposits, and finally a high-energy shoal complex, representing a base-level-fall hemicycle. The large-scale cross-stratification in section 4 is interpreted as a tidal sand wave. Counter-flow ripples, together with minor erosion of single foresets, point to tidal activity. The occurrence of a low-energy facies on top of the sequence corresponds

Table 1 Classification and description of microfacies

Micro-facies number	Microfacies name	Lithology and colour	Components[1]	Bedding	Description and sedimentary structures	Depositional environment and interpretation
1	shell-fragment grainstone and packstone	limestone; light grey or beige	shell debris with micritic envelopes (a), intraclasts (c), coated grains (r-c), ooids (r-c), peloids (r), quartz (r), gastropods (vr)	medium to massive (dm-m)	arenitic to ruditic, well to very well sorted, composed of fragmented shells, amalgamated cross-stratification	shoal complex, exposed to waves and currents
2	shelly ooid grainstone	limestone; light grey or beige	shell debris with micritic envelopes (vc), ooids (vc), coated grains (vc), quartz (r), intraclasts (r),	thin (cm)	arenitic, very well sorted, subhorizontal to low-angle cross-stratification	shoal complex, permanently exposed to waves and currents
3	shelly ooid-layered grainstone and packstone	limestone; light grey or beige	shell debris (a) with prevalent micritic envelopes, ooids (vc), intraclasts (r-c), peloids (r), bivalves (r), brachiopods (r), quartz (vr)	thin to medium (cm-dm)	arenitic to ruditic, moderately well sorted, ooids preferentially arranged in layers and mainly dolomitised, cross-stratification	shoal margin, episodic input from the shoal complex
4	shelly coated grain packstone	limestone; light to dark grey	shell debris (a) with prevalent micritic envelopes, coated grains & ooids (vc), peloids (r-c), intraclasts (r), quartz (r)	thin (cm)	arenitic to ruditic, well sorted, cross-stratification, continuous transition from MF 1	seaward marginal zone of the shoal complex
5	shell-peloidal packstone	limestone; beige or light grey	shell debris (a) with or without micritic envelopes, peloids (vc), intraclasts (r), bivalves (r), brachiopods (r)	medium (dm)	fine ruditic, poorly to moderately sorted, overall fining-upward, largely subhorizontal alignment of components, umbrella structures	storm-wave dominated offshoal area, tempestite, little lateral transport
6	fine-laminated packstone	limestone; dark grey	shell debris (vc), peloids (c-vc), intraclasts (r-c), bivalves (r), coated grains and ooids (vr)	thin to medium (cm-dm)	fine ruditic, hummocky cross-strat., horizontal lamination, gradually passing into (climbing) ripple lamination, reactivation surfaces, graded, top locally gently bioturbated	storm-wave dominated offshoal area, tempestite
7	graded shell packstone	limestone; beige or light to dark grey	shell debris (a), peloids (c), bivalves (r-c), brachiopods (r-c), intraclasts (r), ooids (vr), glauconite (vr)	medium (dm)	ruditic, poorly to very poorly sorted, random orientation of components, several fining-upward sequences (cm), top locally gently bioturbated, umbrella structures	storm-wave dominated offshoal area, tempestite, erosion and redeposition essentially on the spot
8	shell packstone	limestone; light grey or beige	shell debris (c-vc), locally with micritic envelopes, bivalves (c), brachiopods (c), peloids (r)	medium to massive (dm-m)	ruditic, poorly to moderately sorted, selective dolomitisation of shells and matrix common	offshoal, minor storm-wave influence
9	bioturbated wackestone and packstone	limestone; medium to dark grey	shell debris (vc), fecal pellets (c), bivalves (c), brachiopods (c), ophiuroid osicles (r), ooids (vr)	thin to medium (cm-dm)	arenitic to ruditic, poorly sorted, intensive bioturbation, original structures mostly destroyed, ooids mainly dolomitised	offshoal, at least temporary colonisation by organisms
10	bioturbated fecal-pellet wackestone	limestone; medium to dark grey	fecal pellets (vc), shell debris (c-vc), ophiuroid osicles (r)	thin to medium (cm-dm)	arenitic components, poorly sorted, very intensive bioturbation, very well homogenised, nodular layers common	offshoal, permanent colonisation by organisms
11	lime-mudstone	limestone; medium grey	shell debris (vr), bivalves (vr)	thin to medium (cm-dm)	arenitic components enriched in a few layers, nodular structure common, thin argillaceous lime-mudstone layers commonly intercalated	offshoal, episodic input from storm events
12	argillaceous lime-mudstone	argill. limestone; medium to dark grey	none	thin to medium (cm-dm)	fine-laminated argillaceous limestones, intercalations of micritic lime concretions	offshoal, low-energy conditions, argillaceous background sedimentation; in part possibly lagoonal?

[1] a=abundant; vc=very common; c=common; r=rare; vr=very rare

to a base-level rise. This asymmetric sequence is interpreted as the result of a prograding shoal complex followed by a retrogradational phase (Fig. 6a).

Shoal margin genetic sequence

Description: This type of succession reaches an average thickness of 1–1.5 m (Fig. 6b). It commonly starts with lime mudstone and intercalated argillaceous layers. The lime mudstone is sharply overlain by a bioclastic peloidal packstone, typically graded and displaying subhorizontal lamination and umbrella structures (Kreisa 1981). The top is built by cross-bedded grainstones or packstones, which are rich in ooid or shell layers. They show an increase in sorting compared to the lower units. The upper half of the sequence reveals a different pattern, beginning with a bioturbated wackestone or packstone that locally contains winnowed lenses of the underlying lithology at the base. Upwards, bioturbation and the frequency of fecal pellets increase and beds are rather nodular, grading into wackestones and finally lime mudstones. Thin bioclastic packstone layers, commonly with an erosive base and intraclasts, are locally intercalated.

Interpretation: The lower half of the sequence reflects a transition from a quiet depositional environment to a higher energy, shallower setting flanking the shoal complex. The layered accumulations of ooids suggest episodic input from the adjacent shoal complex. In the upper half, microfacies changes and the increasing degree of bioturbation indicate somewhat deeper conditions influenced by storm deposition. This symmetric sequence consists of base-level-fall and -rise deposits of almost equal thickness (Fig. 6b).

Offshoal genetic sequence

Description: This succession is generally 2–3 m thick; the lower part comprises lime mudstone, typically a few decimetres thick, with argillaceous interlayers (Fig. 6c). The lime mudstone is erosively overlain by a complex unit of bioclastic packstones of similar thickness, which in some cases are graded and contain abundant fragmented shells and umbrella structures. In the upper 1.5–2 m, the sequence gradually passes into bioturbated packstones and wackestones and finally into lime mudstones, which again contain several intercalated argillaceous lime mudstone layers, but locally also wackestones or packstones. The sequence usually ends with an argillaceous lime mudstone unit.

Interpretation: Basal lime mudstone represents quiet, sheltered water conditions that pass upward into a storm-influenced offshoal depositional setting, reflecting a fall in base-level. The thicker upper portion of the sequence indicates a deepening-upward trend (base-level-rise hemicycle) expressed by changes in microfacies and increasing clay content. This sequence typically shows an asymmetric organisation (Fig. 6c).

Larger-scale sequences

The genetic sequences form the fundamental building blocks, with regular stacking patterns of larger-scale sequences (Fig. 10).

Description: The lower parts of the studied sections consist of two shoal complex genetic sequences dominated by shallowing-upward portions (asymmetric cycles of base-level fall). They are followed upwards by shoal margin genetic sequences, where deepening-upward portions increase to produce symmetric base-level cycles. This pattern is reflected lithologically by a transition from grainstone-dominated to more packstone-dominated textures, and is also apparent in the outcrop gamma-ray logs.

Interpretation: Based on the stacking pattern analysis, an overall base-level fall can be reconstructed for the lower two genetic sequences, while the following genetic sequences represent an overall base-level rise. The maximum fall in base-level is indicated within the upper shoal complex genetic sequence by shallower, higher-energy conditions. Compared to the lower shoal complex genetic sequence, those conditions produced better rounding and markedly better sorting of the components, as well as an increase in ooids and coated grains. The upper shoal margin genetic sequences reflect overall deepening. The regional study of Braun (2003) proposes that the maximum flooding interval should be placed in the “Hauptterebratelbank”.

Lateral facies successions

The lateral microfacies distribution is very homogeneous on the scale of a kilometre. Variations within particular microfacies types are restricted to differences in composition of a few percent (minimum range 2%, maximum range 9%; Fig. 11). Only one case of noticeable change in microfacies composition was detected in the northernmost outcrop (section 1). In this location, microfacies 1 (shell-fragment grainstone and packstone), which essentially builds the carbonate shoal complex, consists of a higher proportion of micrite and a consequent shift towards more packstone textures. Moreover, microfacies 8 (shell packstone) is far more abundant and comprises a higher percentage of peloids.

The internal structure of genetic sequences shows no other significant changes (Fig. 12). Shoal complex, shoal margin, and offshoal genetic sequences can be correlated laterally without difficulty. Minor variations in thickness of a few decimetres are presumably caused by variations in depositional topography and hydrodynamic processes. This has little influence on the structure of these sequences. Changes in microfacies in section 1 mentioned above are postulated to reflect somewhat lower energy conditions for this location.

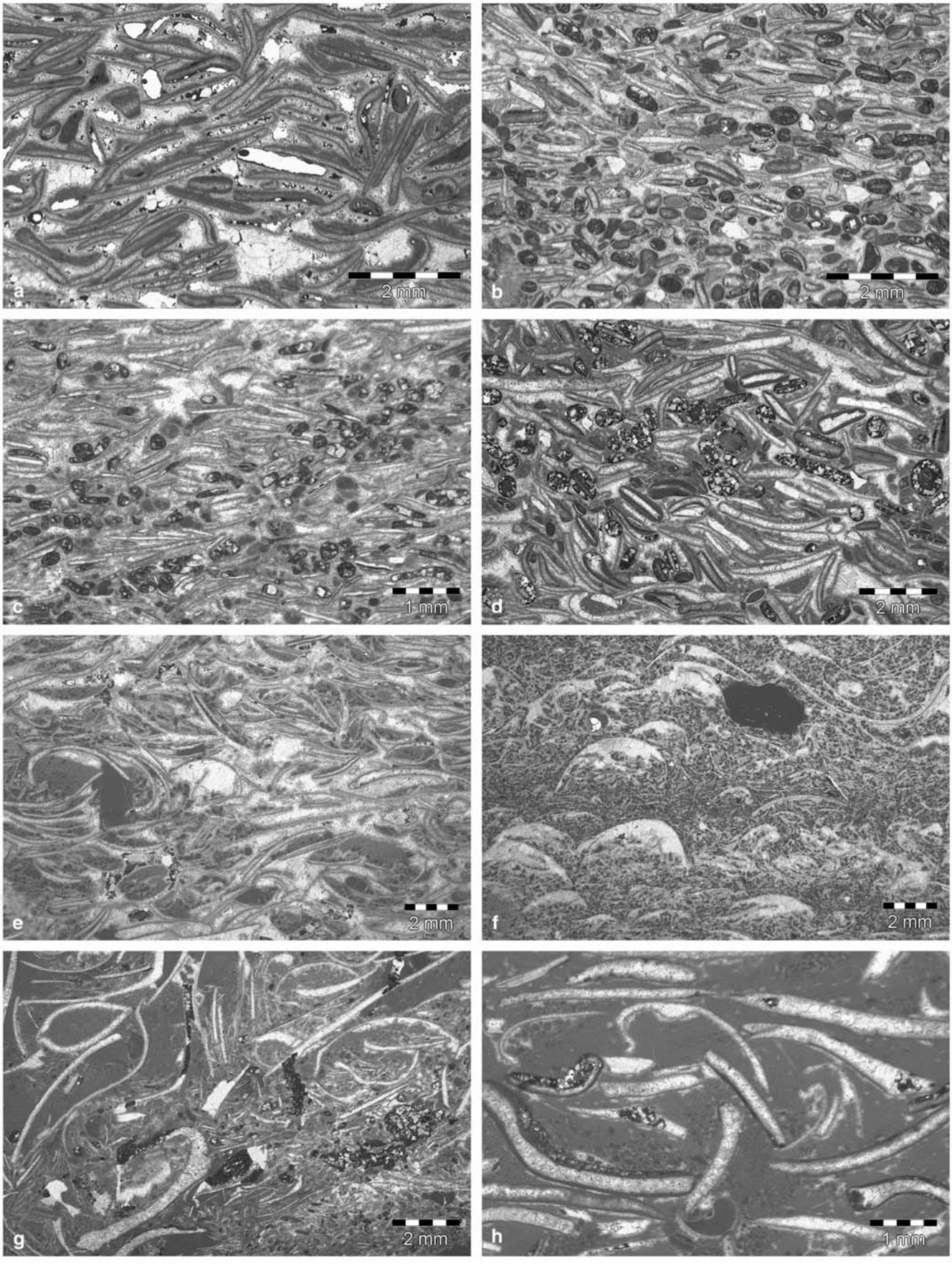
a
2 mm
b
2 mm
c
1 mm
d
2 mm
e
2 mm
f
2 mm
g
2 mm
h
1 mm

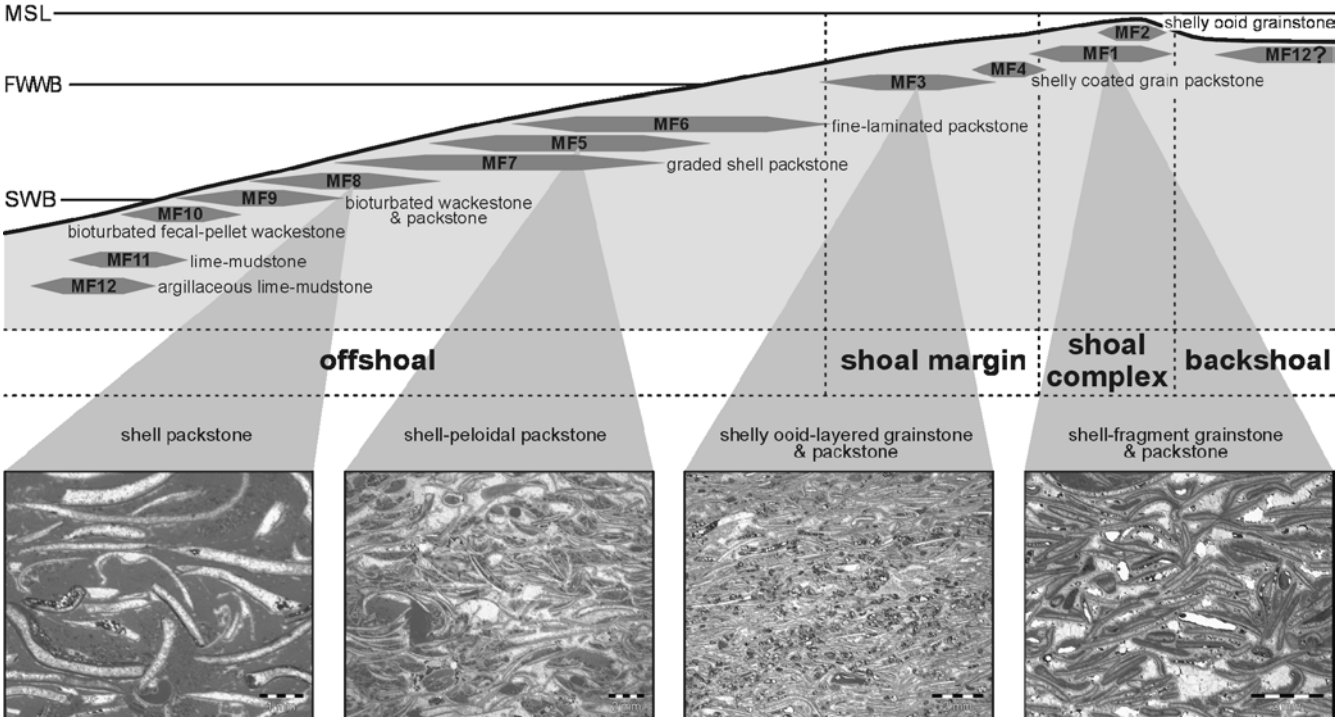

Fig. 5 Interpretation of microfacies distribution along the Upper Muschelkalk carbonate ramp (MSL = mean sea level, FWWB = fair-weather wave base, SWB = storm wave base)

Paleocurrents

Paleocurrent data are mainly derived from the high-energy facies within the shoal complex genetic sequence, by measuring the orientation of trough cross-stratification and wave ripples in three-dimensional exposures.

Wave ripples

Wave ripples occur in fine to medium carbonate sands, but few locations are suitable for measurement. Wave-ripple crests show two main orientations running either perpendicular or parallel to the ancient shoreline, trending roughly southwest-northeast (Fig. 13a). Aigner (1985) interpreted similar paleocurrent patterns in Up-per Muschelkalk (Ladinian) carbonates as the result of dominantly longshore winds and storms coming in from the Tethys to the southwest, which would generate primarily alongshore wave trains in offshore areas. Wave reflection in nearshore shallow-water settings accounts for wave-ripple orientation oblique or parallel to the shoreline.

Fig. 4a–h Plate showing the most prominent microfacies types (MF) of Upper Muschelkalk shoal-water carbonates in Sommerhausen quarry sections. **a** Shell-fragment grainstone (MF 1), predominantly composed of fragmented mollusc shells with micritic envelopes. Section 2 – 2.44 m. **b** Shelly ooid grainstone (MF 2), very well sorted; main components are fragmented shells with micritic envelopes, ooids, and coated grains. Section 3 – 1.17 m. **c** Shelly ooid-layered grainstone (MF 3) with fragmented shells and ooids preferentially arranged in layers. Section 2 – 6.23 m. **d** Shelly coated grain packstone (MF 4), mainly composed of fragmented shells with prevalent micritic envelopes, coated grains, and ooids. Section 2 – 3.75 m. **e** Shell-peloidal packstone (MF 5), characterised by fragmented shells and an abundance of peloids. Umbrella structures are common. Section 4 – 6.17 m. **f** Fine-laminated packstone (MF 6). Fragmented and disarticulated shells, peloids, and intraclasts are the main components; typical horizontal lamination. Section 2 – 1.34 m. **g** Graded shell packstone (MF 7) with abundant fragmented shells; bivalves, brachiopods, and peloids are common. Section 4 – 5.97 m. **h** Shell packstone (MF 8), characterised by fragmented shells, including brachiopods and bivalves, and peloids. Section 2 – 5.25 m

Trough cross-stratification

Paleocurrent measurements were collected from dune trough cross-stratification and, to a lesser degree, from ripple cross-lamination. Data were also taken from cross-stratification of a tidal sand wave and associated counter-flow ripples in section 4. Most foresets dip northeast to northnortheast, pointing to a dominant longshore sand-body migration towards the NE/NNE (Fig. 13b). Few measurements indicate eastward, onshore-directed sand transport, whereas offshore-directed transport was determined only in four measurements at section 3. The tidal sand wave displays alongshore migration towards the northeast. Two counter-flow ripples reveal an opposite movement towards the southwest. Since there is no further evidence of a tidally-driven circulation, only minor tidal activity is postulated. Storm-generated sedimentary structures (hummocky cross-stratification), the

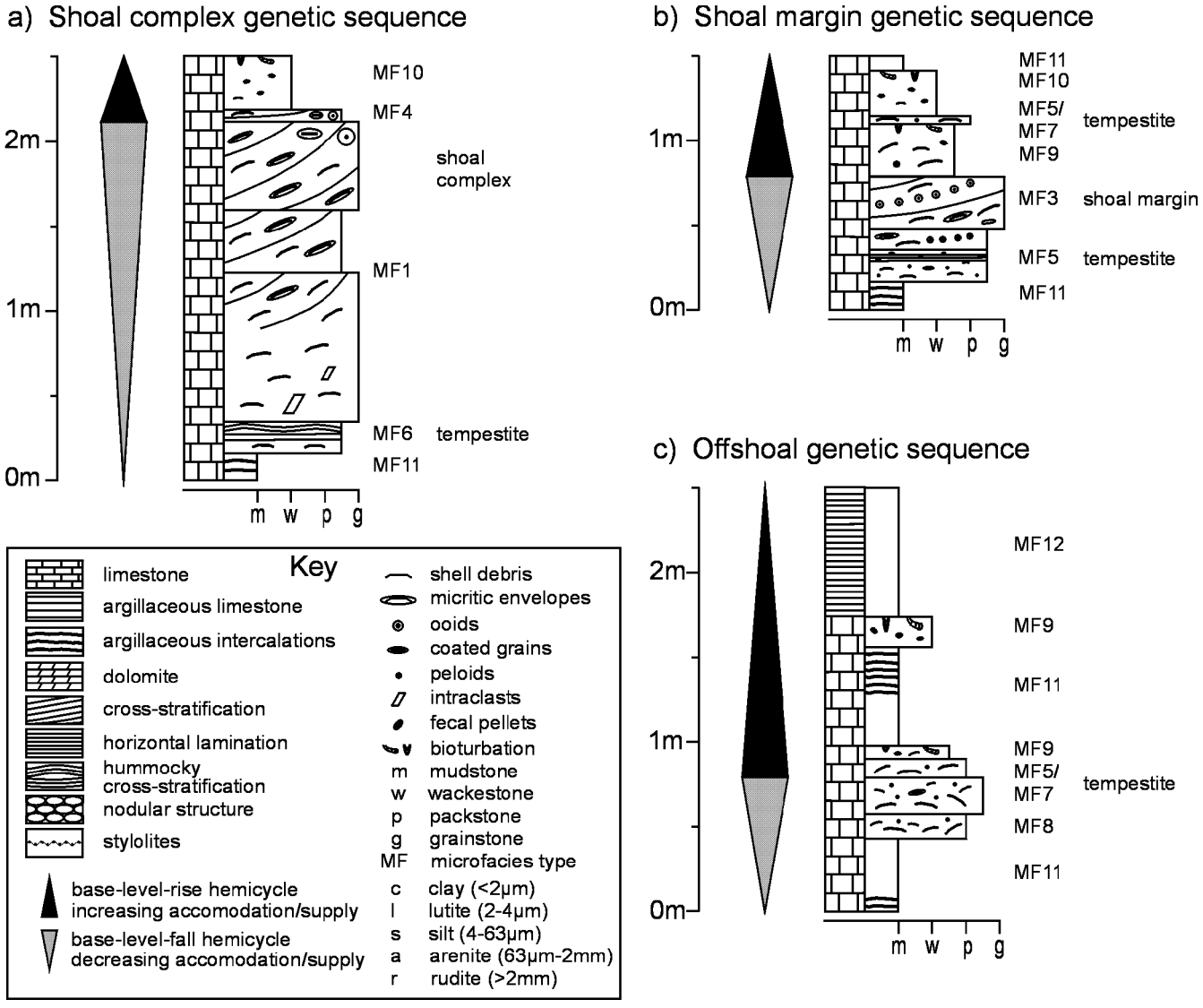

Fig. 6 Generalized logs through a **a** shoal complex genetic sequence, **b** shoal margin genetic sequence and **c** offshoal genetic sequence. A comprising microfacies description is given in Table 1

high degree of amalgamation of cross-bed sets, and correlation of wave-ripple orientation with cross-stratification patterns clearly favours a dominance of a wind- and storm-driven hydraulic regime. In such a regime, longshore sediment transport is attributed to wind-induced alongshore currents. Onshore-directed transport is ascribed to nearshore water set-up during storm events, while backflows of these storm surges are likely responsible for offshore-induced transport. Similar hydrodynamic processes are described from modern studies of the Atlantic shelf of North America (Swift et al. 1983) and from ancient examples of the Upper Muschelkalk (Aigner 1985). Tidal activity is generally most effective when associated with wind-driven currents as reconstructed for the study area. However, major sediment transport is assigned to episodic high-energy storm events.

Fig. 7a–g Plate showing sedimentary structures of shoal-water carbonates in Sommerhausen quarry sections. Scale is 10 cm, except in Fig. 1. **a** Subhorizontal lamination passing into several sets of climbing ripples. Notice the decrease in grain size on moving upward, as indicated by the decrease of lighter (coarser grained) layers. This succession is the result of a waning storm flow. Section 2 – 1.34–1.40 m. **b** Hummocky cross-stratification with characteristic hummocks (antiforms) and swales (synforms). Section 3 – 1.38–1.50 m. **c** Dune trough cross-stratification (dotted) indicating sand migration towards the viewer. Section 3 – 3.90–4.50 m. **d** Ripple lamination is commonly trough cross-stratified when viewed in 3-D exposures like this one. Section 1 – 0.50–1.0 m. **e** Tidal sand wave. Foresets are tangential towards the erosive base and are cut off at the top. Section 4 – 1.50–2.30 m. **f** Counter-flow ripples migrating upwards on foresets of a larger sand wave. Confer with bipolar current measurements for this section in Fig. 13b. Section 4 – 1.80 m. **g** Simplified sketch of Fig. 7f highlighting the sedimentary structures

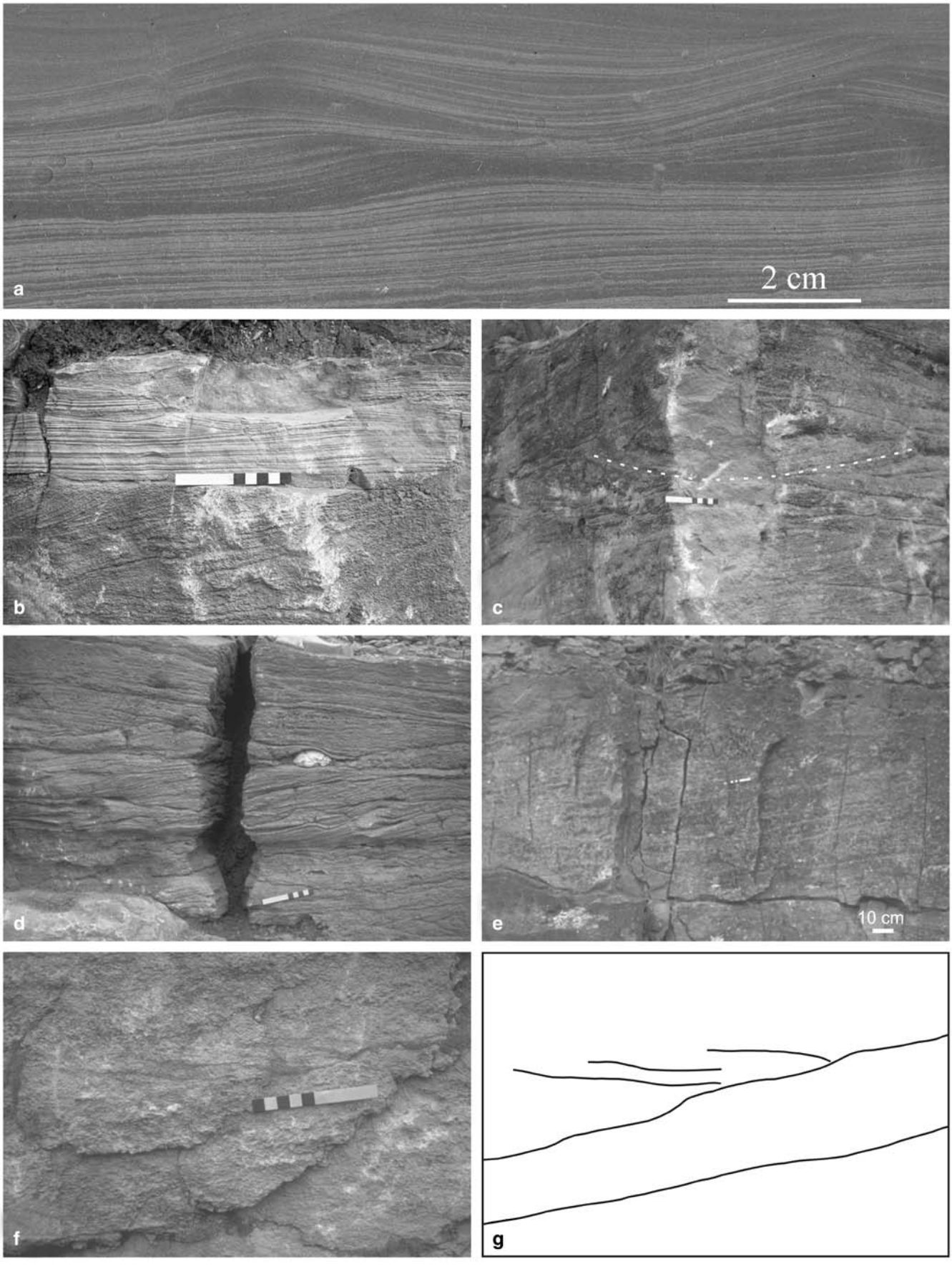
a
2 cm
b
c
d
e
10 cm
f
g

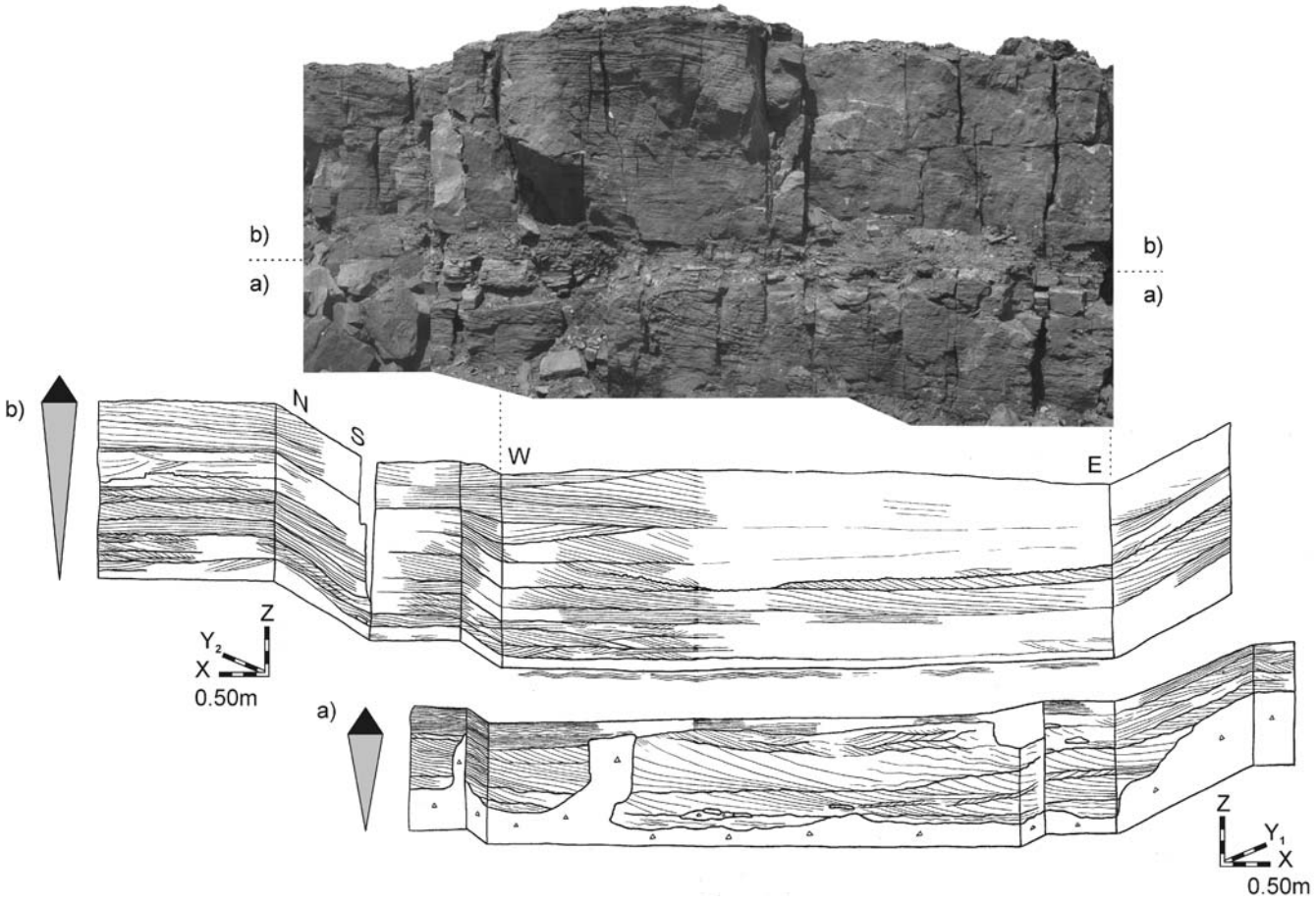

Fig. 8 Sedimentary structures revealed in section 2. Note the dominance of highly amalgamated dune cross-stratification in the course of two shoal complex genetic sequences

Petrophysical reservoir properties

A goal of this study is to document reservoir properties of the Upper Muschelkalk shoal-water carbonates. This account concentrates on the characterisation and spatial distribution of porosity and permeability.

Petrophysical classification

The petrophysical analysis of various microfacies types clearly displays strong variations of porosity and permeability (Fig. 14a). Variations occur not only between microfacies types but also within a single type. This variation is related to different pore structures; so it is necessary to classify pore space in order to define petrophysical classes. The definition of pore space presented by Lucia (1983) emphasises petrophysical aspects, and for that reason was applied in this study. Lucia grouped pore types into pore space located between grains or crystals, called interparticle porosity, and all other pore space, called vuggy porosity. The latter is further subdivided into vugs that are interconnected only through the interparticle pore network, termed separate vugs, and vugs that form an interconnected pore system, termed touching vugs.

Upper Muschelkalk carbonates of the study area show 1) separate vug pore types (dominant), occurring mainly as moldic (dissolved particles) and subordinately as intraparticle pore types, and 2) interparticle pore space, which only becomes important within the high-energy microfacies (type 1; shell-fragment grainstone and packstone) of the shoal complex. Touching vugs in the form of fractures and solution-enlarged fractures appear to be important only in surface outcrops.

The porosity classification of Lucia (1983) is based on the fact that pore-size distribution controls permeability and saturation, and that pore-size distribution is related to rock fabric. Rock fabric is divided into grain- and mud-dominated fabrics (Lucia 1995, 1999), which comprise minor modifications of Dunham's (1962) classification. Grain-dominated fabrics are characterised by a grain-supported texture and the presence of open or occluded intergrain porosity. The important attribute of mud-dominated fabrics is that the areas between the grains are filled with mud even if the grains appear to form a supporting framework. The combination of rock fabric with pore types permits a reasonable petrophysical

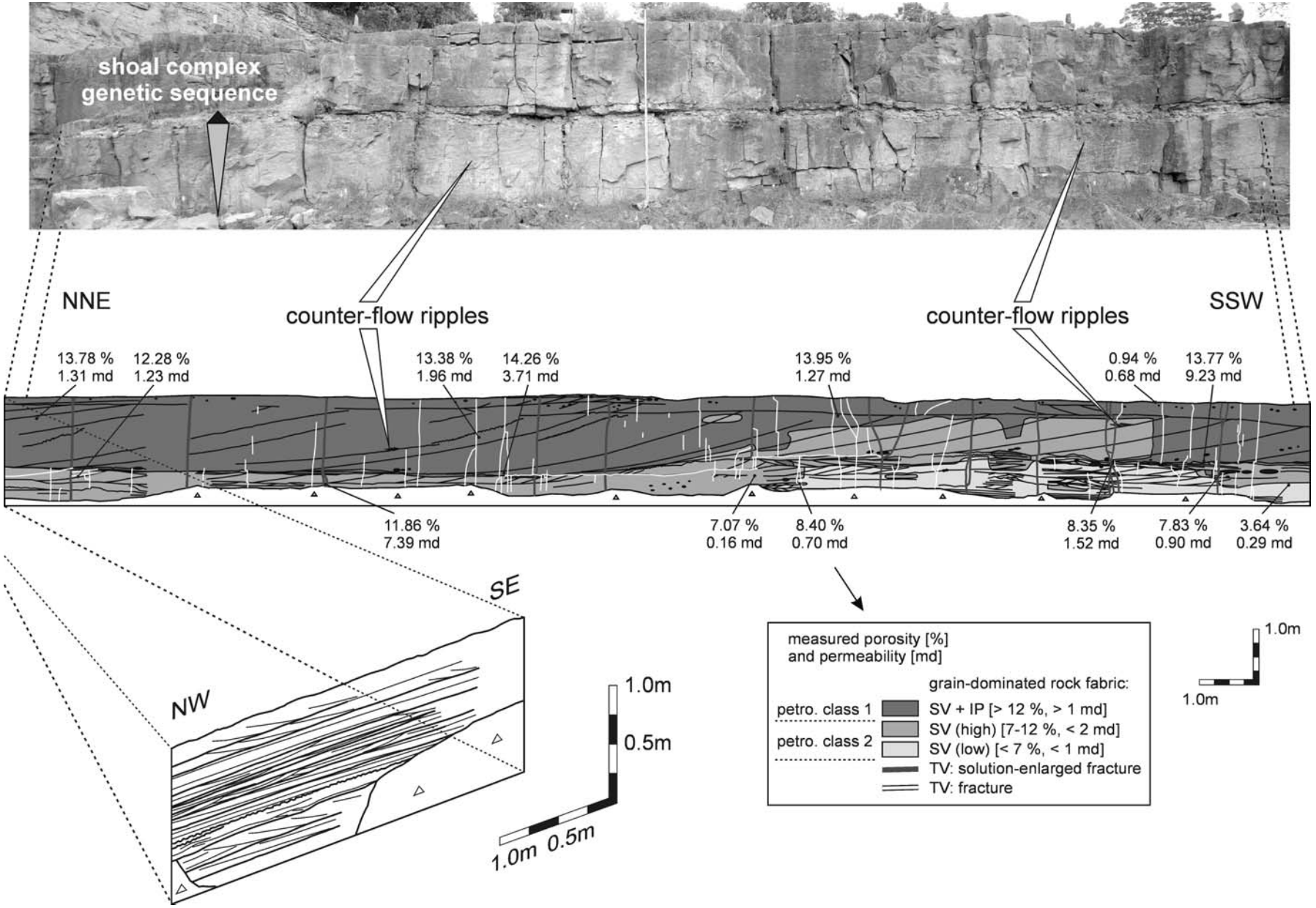

Fig. 9 Tidal sand wave with counter-flow ripples in section 4 where poroperm distribution was measured. Note the upward increase in porosity and permeability during the regressive phase of the shoal complex genetic sequence, and the good lateral continuity of poroperm properties. The trough cross-stratified ripples (enlarged perpendicular section in foreground) migrate upwards along the foresets of the larger sand wave

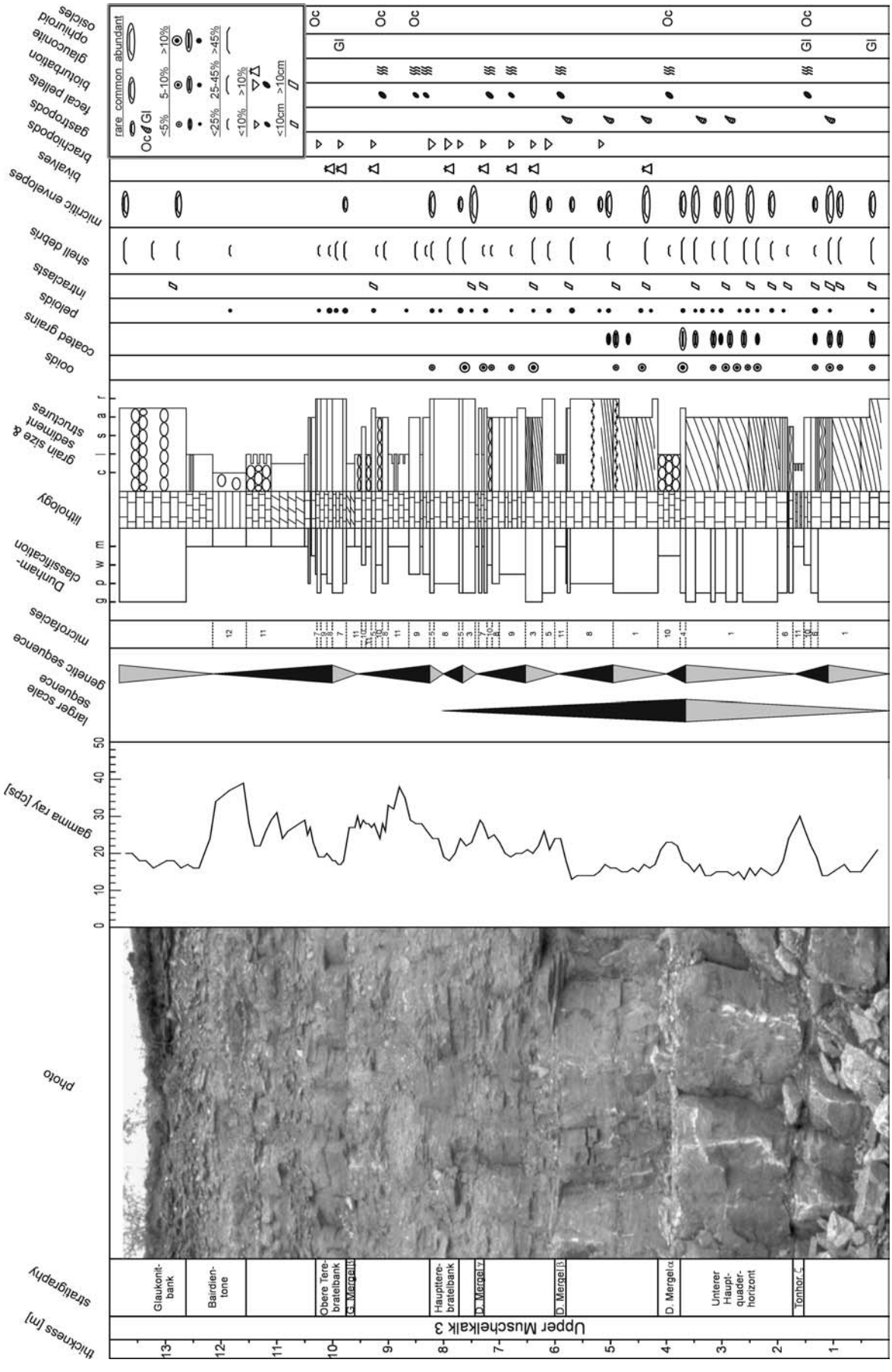

Fig. 10 Vertical facies succession and gamma ray log in section 2. For symbols also refer to key in Fig. 6

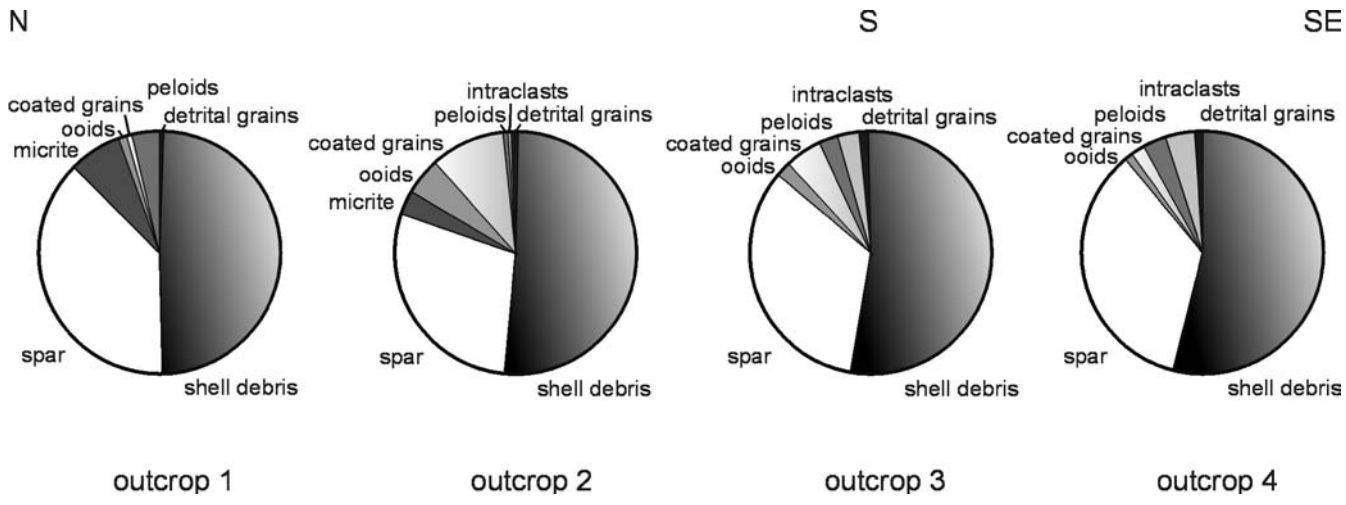

Fig. 11 Lateral variation in composition of microfacies 1 (shell-fragment grainstone and packstone) close to the turnaround from base-level fall to rise for the lower shoal complex genetic sequence. The exact stratigraphic position in each section is marked by a star symbol in Fig. 12

classification. In this way four petrophysical classes were defined for the study area (Fig. 14b). Class 1 represents the best reservoir qualities (ϕ=5–20%, *k*=1–20 md), which is mainly due to the occurrence of separate vug plus interparticle pore space (Fig. 15). Reservoir qualities are poorer in class 2, where only separate vug pore space is present. Significant differences exist between a grain- and mud-dominated rock fabric, as reflected by classes 2 (ϕ=0.5–12%, *k*=0.3-2 md) and 3 (ϕ=0.5–5%, *k*=0–0.3 md). Class 4 includes non-reservoir rocks (ϕ=0–0.5%, *k*=0–0.1 md). Low porosity and permeability values of class 4 samples with a grain-dominated rock fabric are due to the closing of formerly connected pore space by cementation. Incorporating Dunham textural classes does not allow further subdivision of petrophysical classes. It can be concluded that, within a grain-dominated rock fabric, isolated pockets of micrite alter petrophysical properties only slightly, meaning that this micrite petrophysically resembles components rather than matrix.

Sorting and grain size also have an important effect on petrophysical properties (Fig. 16). Within a petrophysical class, a decrease in grain size and an increase in sorting generally leads to higher porosity values, given constant permeability values. This relationship is a result of variations in size and distribution of pore space.

Spatial distribution of petrophysical parameters

The spatial distribution of porosity and permeability is best described within the cyclic framework. The occurrence of petrophysical classes in a sequence depends on the distribution of petrophysically-related rock properties such as rock fabric and pore type. The vertical and lateral succession of rock properties can be used to predict reservoir qualities of Upper Muschelkalk carbonates.

Within the genetic sequences, an upward increase of porosity and permeability is generally observed in shallowing-up (base-level-fall) hemicycles. The values decrease considerably in subsequent deepening-up (base-level-rise) hemicycles. This general trend differs quantitatively in the various genetic sequences. As expected, by far the best petrophysical properties (ϕ=0.3–20%, *k*=0.2–53 md) are recorded in the shoal complex genetic sequences composed predominantly of classes 1 and 2. The shoal margin genetic sequences are generally characterised by classes 2 and 3 (ϕ=0.05–11.5%, *k*=0.04–5.6 md), while offshoal genetic sequences consist of class 4 and very rarely of classes 2 and 3 (ϕ=0–2.5%, *k*=0–1.4 md).

Horizontal permeabilities are often up to two times greater than vertical permeabilities, which is attributed to sedimentary structures and the alignment of particles, particularly fragmented shells, typically parallel to those structures (see Fig. 12).

Lateral variations of porosity and permeability on an outcrop-scale are generally low (see Fig. 9), except where touching-vug pore space (fractures) forms a vertically-connected pore system. Using the methods of this study, it was not possible to measure to what extent fractures alter porosity and permeability, and how far they expand into the subsurface. The lateral distribution of petrophysical parameters for the whole study area shows a trend from highest porosities and permeabilities in the more southerly-located outcrops to slightly lower values in the northernmost section (Fig. 12). This is consistent with the increase of depositional energy in a southward direction, as proposed for the sedimentary environment.

The distribution of petrophysical parameters within the genetic sequences displays an overall trend. It is expressed by a systematic increase of porosity and permeability towards the regressive maximum of the larger-scale sequence (porosities up to 20% and permeabilities up to 53 md), followed by a decrease in the subsequent

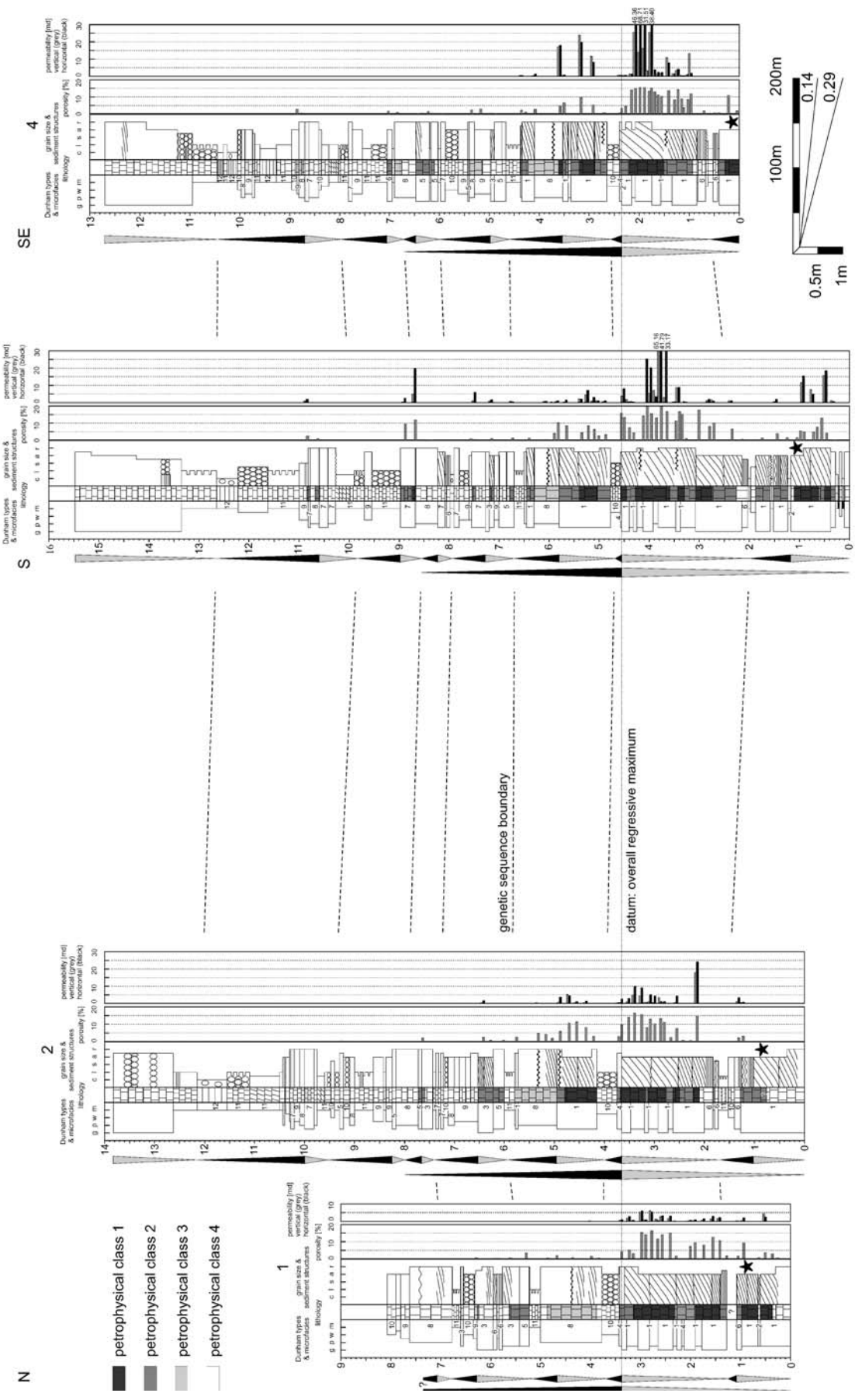

Fig. 12 Correlation of sections 1 through 4 (for location see Fig. 1). The high degree of correlation is also expressed in the porosity and permeability distribution that display maximum values close to the overall regressive maximum. A star symbol represents the stratigraphic position of microfacies type 1 illustrated in Fig. 11. For symbols refer to the key in Fig. 6

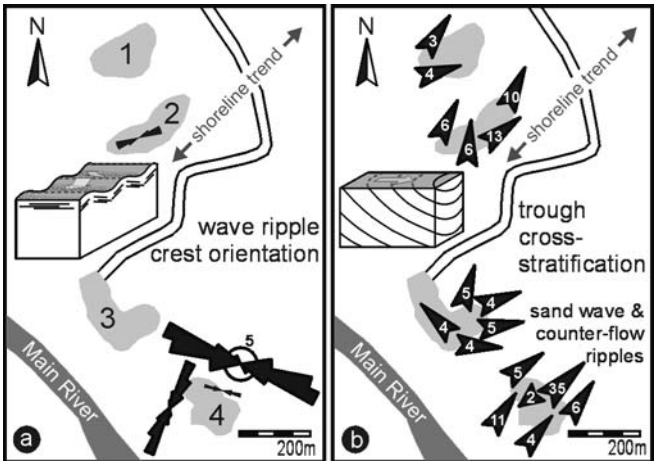

Fig. 13 Paleocurrrent measurements derived from the high-energy facies of the shoal complex (see Fig. 1 for location). **a** Wave-ripple orientation in sections 2 and 4 indicate oscillatory flow parallel and perpendicular to the ancient shoreline (Fig. 2). **b** Trough cross-stratification measurements indicate mostly longshore (NE-directed), but also onshore- and offshore-directed sand transport (section 3). Notice the opposite orientations of the tidal sand wave (NE-directed) and counter-flow ripples (SW-directed) in section 4. Numbers indicate quantity of measurements

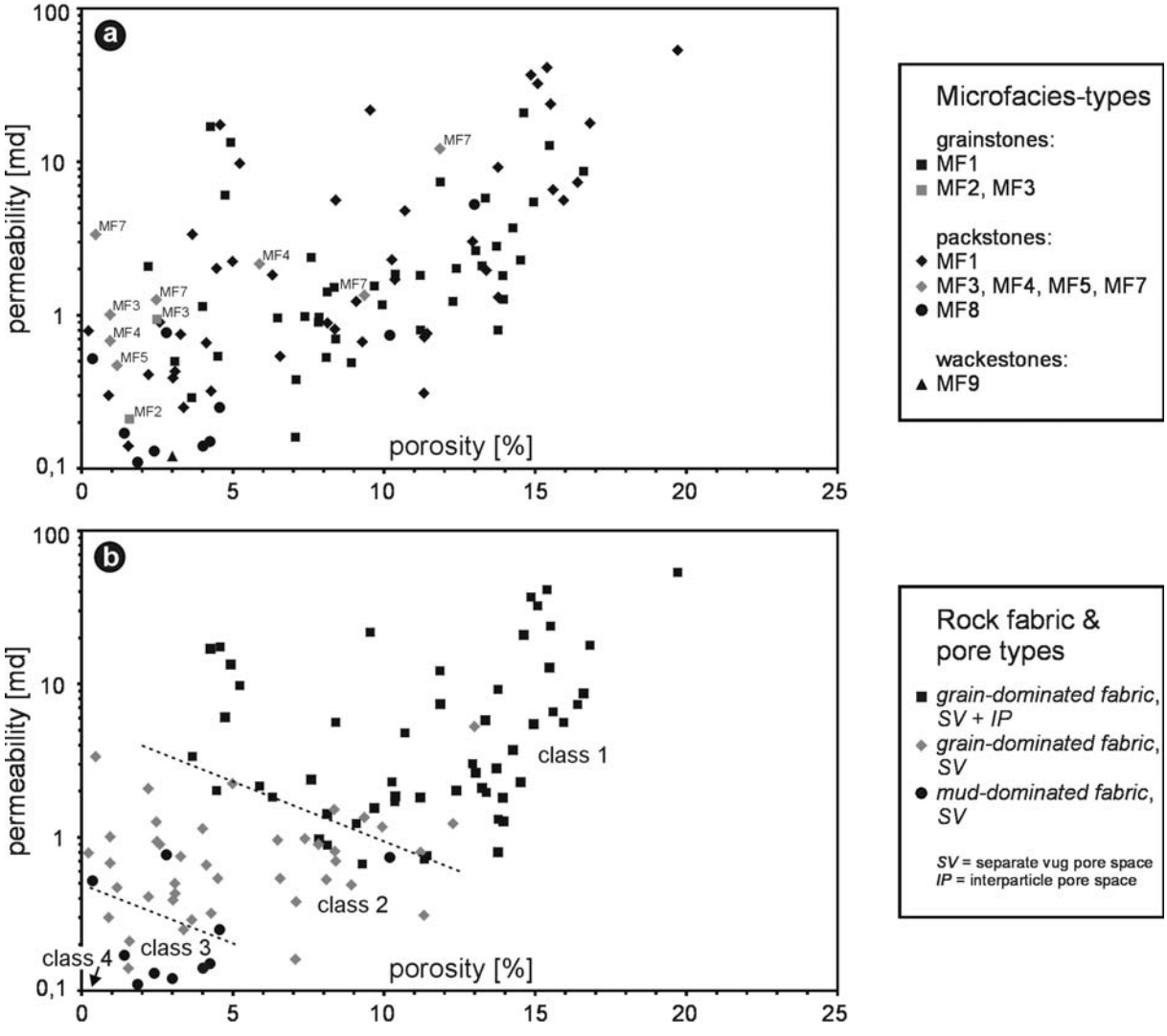

Fig. 14 Porosity-permeability cross plot based on **a** microfacies, showing strong variations between different types as well as within single types, and **b** rock fabric and pore types, that allow differentiation of petrophysical classes. Grain-dominated fabrics are grainstones and packstones of Dunham (1962), that have intergrain pore space or cement; mud-dominated fabrics are packstones, wackestones and mudstones whose intergrain spaces are filled with mud (after Lucia 1995, 1999). Interparticle pore space (pore space located between grains or crystals) and separate vug pore space (all other pore space which is interconnected only through the interparticle pore network) of Lucia (1983) are classified as fabric selective pore types of Choquette and Pray (1970)

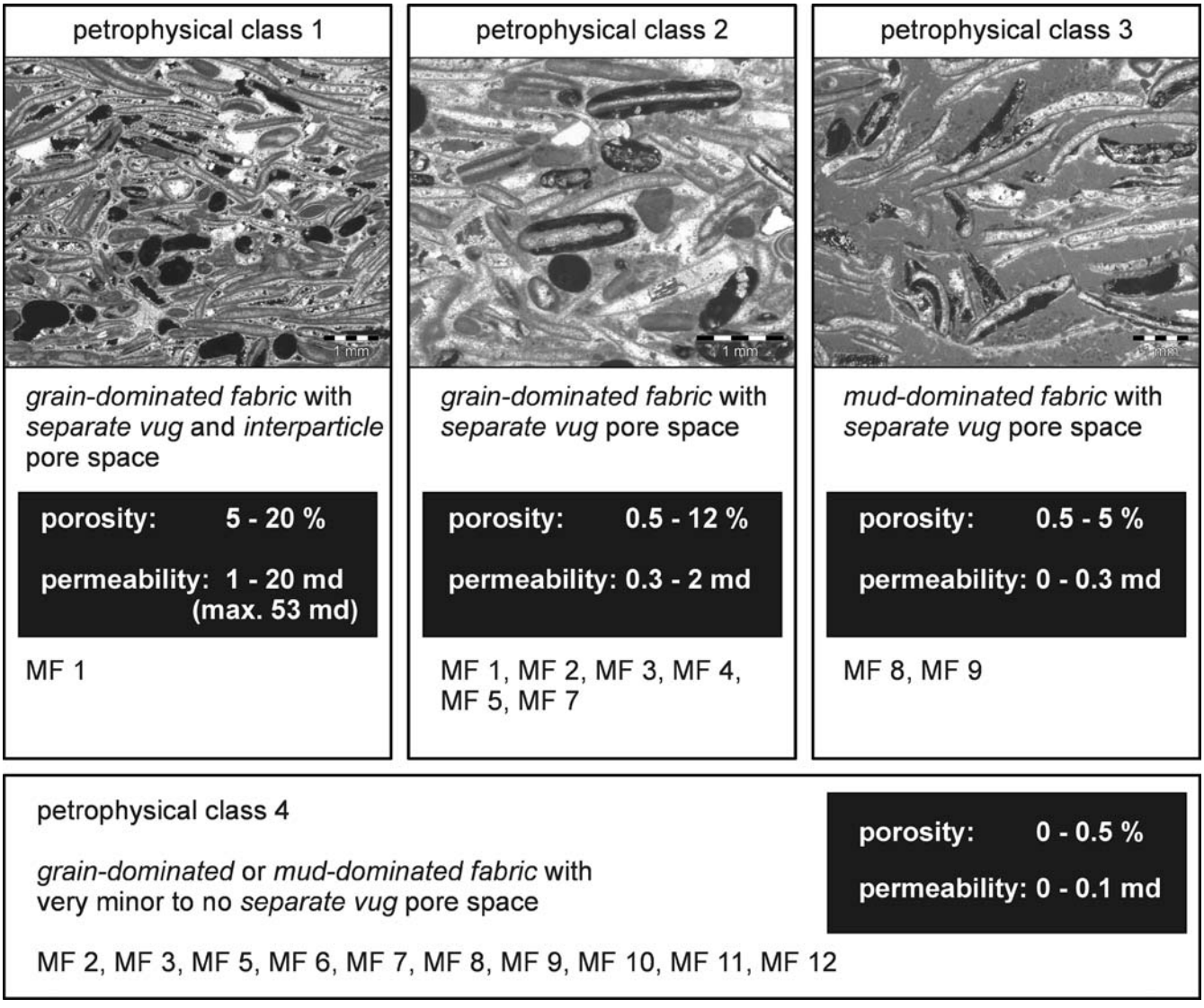

Fig. 15 Petrophysical classes according to rock fabric and pore types (for further explanation refer to text and Fig. 14). Black areas in photographs highlight the pore space (observations under crossed polars)

overall transgression. In addition, the thickness of potential reservoir rocks increases towards the overall regressive maximum (Fig. 17). In terms of reservoir geometry, the studied area represents a layer-cake structure with laterally continuous fluid-flow units.

Conclusions

The sedimentary and poroperm anatomy of Upper Muschelkalk shoal-water carbonates was analysed, and yielded the following data:

1. Microscopic analysis showed several high-energy-shoal facies types, tempestites, and lower energy carbonates, and was used to characterise petrophysical properties.
2. Sequence analysis revealed a cyclic organisation of the Upper Muschelkalk carbonates in 1–3 m thick genetic sequences. Correlation of genetic sequences within a kilometre is excellent, and changes in microfacies composition are restricted to a few percent. Several genetic sequences stack to form larger-scale regressive and transgressive trends.
3. Because of the strong variations of petrophysical parameters between different microfacies, as well as within single microfacies types, a reasonable petrophysical characterisation cannot be based on microfacies. By incorporating rock fabric with pore types supported by quantitative measurements of porosity and permeability, four significant petrophysical classes were determined.
4. The macroscopic distribution of poroperm parameters on an outcrop-scale is determined by genetic sedimentary sequences, and reflects primary energy con-

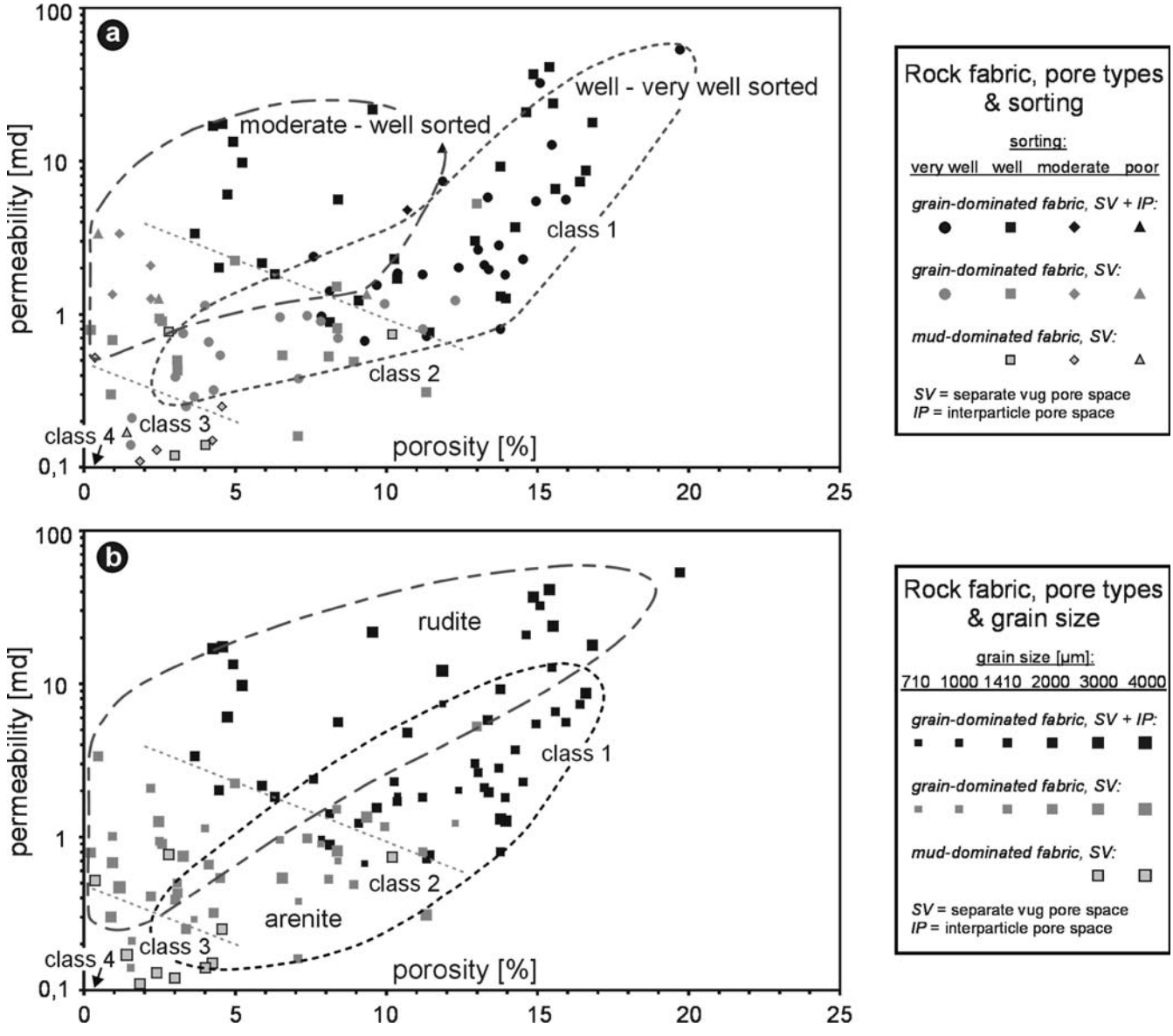

Fig. 16 Cross plot showing the importance of **a** sorting and **b** grain size on the porosity and permeability

ditions during deposition. Porosity and permeability show only minor lateral variations within single layers. Vertically, they generally increase in the course of a regressive phase and significantly decrease during subsequent transgressive phases.

5. The thickest reservoir bodies (up to 2 m) with the best reservoir qualities (ϕ up to 20%, *k* up to 53 md) occur during the peak of the large-scale regressive maximum.
6. The thickness of potential reservoir rocks varies only slightly in the study area, therefore exhibiting a layer-cake geometry with laterally continuous poroperm properties.

The high degree of lateral facies and poroperm continuity on a scale of 1300 m may be important for subsurface reservoir modelling, where often only limited well data are available. As documented here, shallow-ramp shoal-water complexes can be expected to exhibit facies and poroperm continuity on a scale greater than a kilometre.

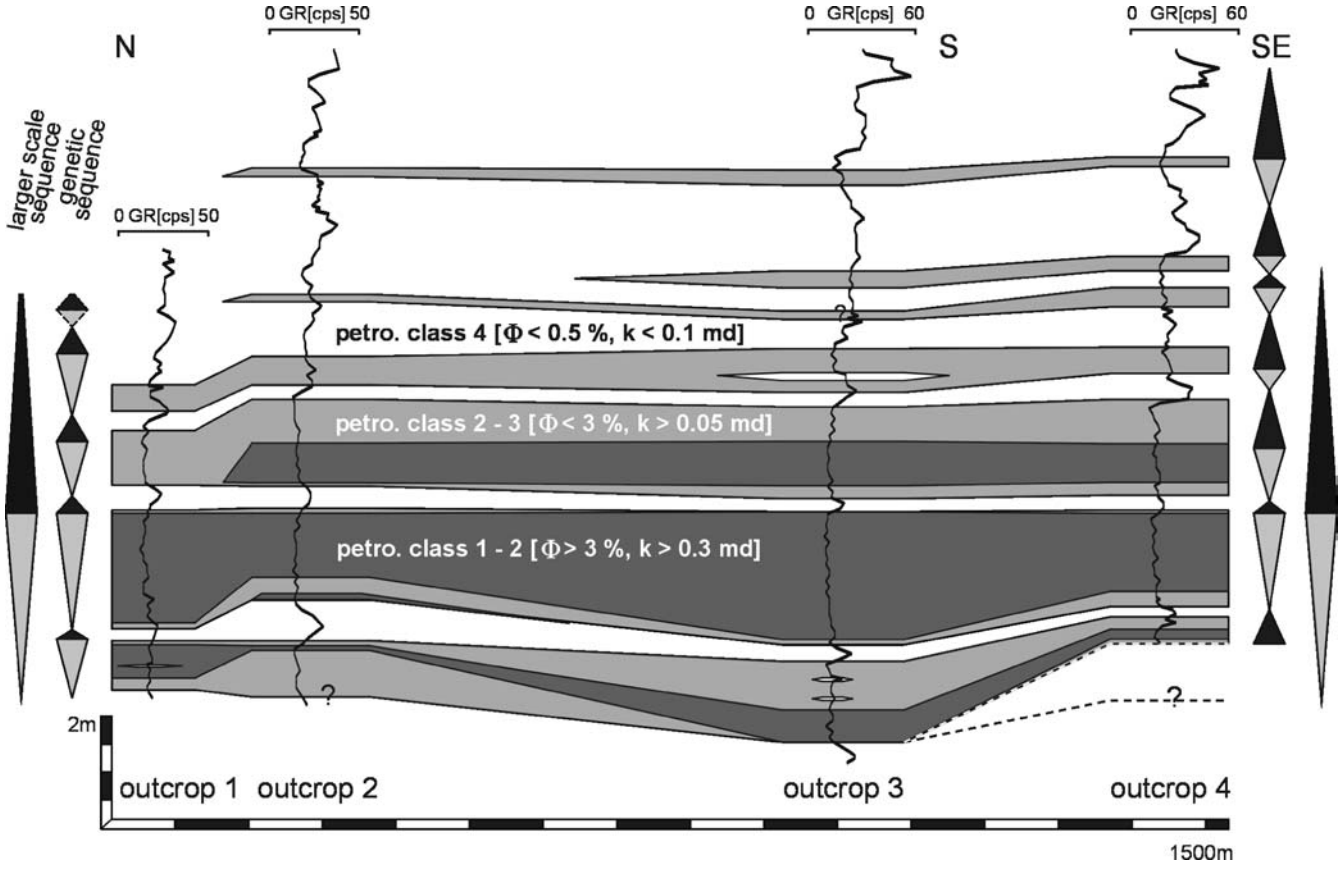

Fig. 17 Reservoir model showing geometry and thickness of potential reservoir rocks within the sequence stratigraphic context. The reservoir is characterised by laterally continuous fluid flow units (shaded) that increase in thickness towards the overall regressive maximum. Dark grey = best reservoirs (petrophysical classes 1–2), light grey = moderate-good reservoirs (petrophysical classes 2–3), white = non-reservoir (petrophysical class 4). Note that the outcrop gamma-ray logs do provide a good first approximation of reservoir distribution

Acknowledgements We gratefully appreciate the helpful comments of P. Enos and F.J. Lucia who reviewed this paper. R. Borkhataria and J. Titschack are thanked for constructive comments on an earlier version of the manuscript. We want to further thank the quarry operators, Renninger Steinbruch-Erdbau, for giving us permission to access their sites.

References

Aigner T (1985) Storm depositional systems. Dynamic stratigraphy in modern and ancient shallow-marine sequences. Lec Notes Earth Sci 3, Springer, Berlin Heidelberg New York, p 174

Aigner T, Heinz J, Hornung J, Aspiron U (1999) A hierarchical process-approach to reservoir heterogeneity: examples from outcrop analogues. Bull Centre Rech Elf Explor Prod 22(1):1–11

Braun S (2003) Quantitative analysis of carbonate sandbodies: outcrop analog study from an epicontinental basin (Triassic, Germany). PhD Thesis (unpubl), University of Tübingen, Tübingen, Germany, p 93

Busch DA (1959) Prospecting for stratigraphic traps. AAPG Bull 43(12):2829–2843

Choquette PW, Pray LC (1970) Geologic nomenclature and classification of porosity in sedimentary carbonates. AAPG Bull 54(2):207–250

Cross TA, Lessenger MA (1998) Sediment volume partitioning: rationale for stratigraphic model evaluation and high-resolution stratigraphic correlation. In: Sandvik KO, Gradstein F, Milton N (eds) Predictive high resolution sequence stratigraphy. Nor Petrol Soc Spec Publ 8:171–196

Dott RH, Bourgeois J (1982) Hummocky stratification: Significance of its variable bedding sequence. Geol Soc Am Bull 93:663–680

Dunham RJ (1962) Classification of carbonate rocks according to depositional texture. In: Ham WE (ed) Classifications of carbonate rocks. AAPG Mem 1:108–121

Hagdorn H (ed)(1991) Muschelkalk: a field guide. Goldschneck, Korb, Germany, p 21

Homewood P, Guillocheau F, Eschard R, Cross TA (1992) Corrélations haute résolution et stratigraphie génétique: une démarche intégrée. Bull Centre Rech Elf Explor Prod 16:357–381

Homewood P, Mauriaud P, Lafont F (2000) Best practices in sequence stratigraphy for explorationists and reservoir engineers. Bull Centre Rech Elf Explor Prod Mem 25:81

Kozur H (1974) Biostratigraphie der germanischen Mitteltrias. Freib Forschungsh C 280(1):1–56; 280(2):1–70

Kreisa RD (1981) Storm-generated sedimentary structures in subtidal marine facies with examples from the Middle and Upper Ordovician of Southwest Virginia. J Sediment Petrol 51:823–848

Lucia FJ (1983) Petrophysical parameters estimated from visual descriptions of carbonate rocks: a field classification of carbonate pore space. J Petrol Technol 35(3):629–637

Lucia FJ (1995) Rock-fabric/petrophysical classification of carbonate pore space for reservoir characterization. AAPG Bull 79(9):1275–1300

Lucia FJ (1999) Carbonate reservoir characterization. Springer, Berlin Heidelberg New York, p 226

Matthews RK (1984) Dynamic stratigraphy, 2nd edn. Prentice-Hall, Englewood Cliffs, NJ, p 489

Ruf M (2001) Facies distribution, petrophysics and mapping of selected carbonate sand bodies in the Upper Muschelkalk, South-German Basin: a reservoir analogue investigation. Diploma Thesis (unpubl), University of Tübingen, Tübingen, Germany, p 109

Schröder B (1967) Fossilführende Mittlere Trias im Ries. Geol Bl NE-Bayern 17:44–47

Swift DPJ, Figueiredo AG, Freeland GL, Oertel GF (1983) Hummocky cross-stratification and megaripples: a geological double standard. J Sediment Petrol 53:1295–1317

Urlichs M (1993) Zur Gliederung des Oberen Muschelkalks in Baden-Württemberg mit Ceratiten. In: Hagdorn H, Seilacher A (eds) Muschelkalk-Schöntaler Symposium 1991. Goldschneck, Korb, Germany, 153–156

Urlichs M, Mundlos R (1987) Revision der Gattung Ceratites De HAAN 1825 (Ammonoidea, Mitteltrias). J. Stuttgarter Beitr. Naturk. B 128:36

Wheeler HE (1964) Baselevel, lithosphere surface, and time-stratigraphy. Geol Soc Am Bull 75:599–610

Ziegler PA (1990) Geological atlas of western and central Europe, 2nd edn. Shell Int Petrol M, Den Haag, The Netherlands, p 239